J. Fluid Mech. (2006), *vol.* 554, *pp.* 259–270.
doi:10.1017/S0022112005007974 Printed in the United Kingdom

Raining into shallow water as a description of the collapse of a column of grains

By E. LARRIEU[1], L. STARON[2] AND E. J. HINCH[2]

[1]Institut de Mécanique des Fluides de Toulouse, UMR CNRS/INPT/UPS 5502, 2, Allée du Professeur Camille Soula, 31400 Toulouse, France

[2]Department of Applied Mathematics and Theoretical Physics, University of Cambridge, Wilberforce Road, Cambridge CB3 0WA, UK

(Received 22 February 2005 and in revised form 19 August 2005)

A modified shallow-water model is presented for the collapse of tall columns of grains. The flow is divided in two parts. Depth-averaged shallow-water equations are applied to a thin horizontally spreading layer which is subjected to Coulombic friction. The falling mass of grains is gradually added to the zone of the initial column during the free-fall time of the column. This 'rain' is assumed to have no horizontal momentum. The results obtained here are in agreement with both planar and axisymmetric experiments over a range of aspect ratio a. In particular, the runout distance is found to vary as $a^{0.65}$ (planar) and $a^{0.52}$ (axisymmetric). The flow dynamics compares well with discrete simulations which have been successfully compared with experiments.

1. Introduction

Flows and spreading of granular mixtures are a central problem in geophysics and risk assessment. Real geophysical flows such as rock avalanches and dry debris flows involve materials of great complexity: rocks of various sizes and shapes, unconsolidated soils, and ashes. Many features of such flows can be reproduced in small-scale experiments using model granular materials. These allow for a better understanding of the dynamics of natural flow and provide a basis for the improvement of continuum models.

In geophysical flows, such as landslides or pyroclastic flows, the prediction of the runout is crucial for hazard prevention. Collapse and spreading of two-dimensional and cylindrical columns of grains onto a horizontal plane have been recently investigated in laboratory experiments to characterize better this runout distance (Lube *et al.* 2004; Lajeunesse, Mangeney-Castelnau & Vilotte 2004). In these experiments, the flow is only driven by the collapse and is highly unsteady. The most striking result is that the runout distance depends only on the initial geometry of the column and not on the size and type of grain. If h_0 and r_0 are the initial height and the initial radius of the column respectively, and $a = h_0/r_0$ is the initial aspect ratio, then the runout distance r_∞ obeys the following relations for cylindrical columns:

$$\frac{r_\infty - r_0}{r_0} \propto \begin{cases} a & \text{for } a < a_0, \\ a^{1/2} & \text{for } a > a_0, \end{cases} \tag{1.1}$$

where Lube *et al.* (2004) found $a_0 = 1.7$ and Lajeunesse *et al.* (2004) found $a_0 = 0.74$. In this paper, we aim to reproduce these experimental scaling laws in the case of tall columns ($a > 2$) using a shallow-water approach. The case of squat columns ($a < 2$) has

already been studied with the shallow-water equations by Mangeney-Castelnau *et al.* (2004).

A depth-averaged continuum model for the flow of granular material was first introduced by Savage & Hutter (1989) to describe avalanches on inclines. This model with a constant basal friction coefficient was successfully applied (Gray, Wieland & Hutter 1999) to predict the motion of granular material on steep slopes in two and three dimensions. Pouliquen & Forterre (2002) introduced a more sophisticated friction law to reproduce the motion of a granular mass on a rough inclined plane. Yet in the highly unsteady case of a column collapsing due to its own weight, this model fails to recover the behaviour observed experimentally at large aspect ratios. In particular the runout distance obtained scales with h_0/μ, and this overestimates the real runout. This failure is not surprising as the initial aspect ratio of the column does not satisfy the shallow-water hypothesis. Moreover, the vertical fall of the grains and their collision with the bottom plane and underlying grains is a source of important dissipation, which cannot be accounted for by the classical shallow-water equations, where basal friction is the only source of dissipation.

This paper presents a new approach using shallow-water equations. The flow is divided in two parts. Shallow-water depth-averaged equations are applied to the horizontally flowing layer of material which is subjected to Coulombic friction. Material is gradually added to the flow during a time corresponding to the free-fall of the column. This 'rain' is assumed to have no horizontal momentum. By adding mass gradually, the input of potential energy into the system is much lower than the initial energy of the full column. This takes into account the energy dissipated during the collapse. The modified model reproduces over a large range of aspect ratio a the experimental scaling laws for the runout distance and final height in both planar and axisymmetric geometries. In addition it gives satisfactory results for the dynamics of the flow.

At the same time, discrete simulations have been carried out in planar geometry. They reproduce the experimental observations for the column collapse (Staron & Hinch 2005), while giving a powerful insight into the internal structure of the flow. Shallow-water results are compared to these simulations. Comparisons of the dynamics of the flow show good agreement, especially when the flow develops away from the initial region.

2. Raining into shallow water

2.1. *Modelling*

Experimental observations show that the flow can be divided in two parts. While a thin layer of material spreads horizontally, the column collapses in the central region and feeds the flow. Depth-averaged equations can thus be used to describe the spreading dynamics, while the addition of mass to the flow due to the collapse of the column should also be included.

We wish to reproduce the spreading resulting from the collapse of a column of grains of initial radius r_0 and initial height h_0. Being in a dense flow regime, we assume that the flow is incompressible and of constant density ρ (Savage & Hutter 1989). Moreover, we assume a plug-flow velocity profile.† The initial condition consists

† There are experimental indications that the velocity profile is not a plug flow. Within the shallow-water equations one cannot find the evolution of the vertical profile of the velocity, but only the evolution of the horizontal variation of the depth-averaged velocity. We hope this crude level of description is sufficient to give the correct qualitative features of the runout.

of a squat cylinder of initial height h_i and of radius r_0, such that $h_i = 0.1r_0$. To model the increase of mass flowing in due to the column collapse, we add over the course of time a volume flux per unit area

$$q(r,t) = \begin{cases} gt & \text{for } 0 \leqslant r \leqslant r_0, \\ 0 & \text{for } r > r_0 \end{cases}$$

to the initial cylinder during a time interval corresponding to the free-fall of the column, namely for $0 \leqslant t \leqslant t_f$ with $t_f = \sqrt{2(h_0 - h_i)/g}$ (Staron & Hinch 2005). Hence we will use the mass conservation equation:

$$\frac{\partial h}{\partial t} + \frac{1}{r}\frac{\partial (ruh)}{\partial r} = q \tag{2.1}$$

for the axisymmetric case and omitting the two metric factors of r in the planar case, where $h(r,t)$ is the local thickness and $u(r,t)$ the depth-averaged velocity.

The momentum equation is given by

$$\frac{\partial (hu)}{\partial t} + \frac{1}{r}\frac{\partial (rhu^2)}{\partial r} = -\frac{1}{2}Kg\frac{\partial (h^2)}{\partial r} - \mu gh, \tag{2.2}$$

again for the axisymmetric case and omitting the two metric factors of r in the planar case. Note that there is no term qu on the right-hand side, because we are assuming that the mass is added with zero addition horizontal momentum.

The spreading term $-Kgh\,\partial h/\partial r$ is proportional to the material slope. The earth-pressure coefficient K represents the ratio between the horizontal and vertical normal stresses and is related to internal friction. It can be calculated in quasi-static deformations following the standard Mohr–Coulomb plasticity model (Savage & Hutter 1989). In shallow-water modelling of granular flows on inclined planes, both Gray, Tai & Noelle (2003) and Pouliquen & Forterre (2002) observed a better agreement with experimental results when using the hydraulic assumption $K = 1$. We therefore set $K = 1$ in the following.

The frictional term $-\mu gh$ is the shear stress at the base and is proportional to the vertical normal stress. The friction coefficient μ will be assumed to be constant, as in Gray *et al.* (2003) or in Mangeney-Castelnau *et al.* (2004). Its value was calibrated to optimize the comparison with discrete simulations results, and is set to 0.45. The precise value does not affect the general behaviour, only the numerical coefficients. For the simple history of the flow we are considering, we can assume that when the flow stops at some location, it remains stationary there and a reduced value of the friction force is able to resist the spreading term, i.e. we do not include the possibility of the flow restarting or reversing.

2.2. *Numerical method*

The equations are non-dimensionalized using r_0 and $t_0 = \sqrt{2r_0/g}$. Although K and μ could be scaled out of the problem, they are the coefficients through which the internal and basal friction appear in the model so they will be kept in the equations. A simple numerical code has been developed and validated to solve this problem. More refined numerics solving the classical depth-averaged equations can be found in Tai *et al.* (2002) or Mangeney-Castelnau *et al.* (2004).

A standard Eulerian shock-capturing method based on a first-order Roe solver is used to solve the conservative system of variables h and uh (Hirsch 1988). Keeping to a first-order scheme enables this simple model to cope with the shock waves generated through the addition of mass with no further numerical refinements.

The typical grid has 1000 points with $\Delta t = 10^{-3}$. The use of an Eulerian grid without any front tracking implies the absence of any real 'dry zone' where the thickness of the flow is zero. There always exists a steady prelayer of negligible thickness $\epsilon = 10^{-7}$ in which u is set to zero. We have checked that this prelayer has a negligible effect on the behaviour as long as $\epsilon \leqslant 10^{-3} r_0$.

With $\mu = 0$ and no mass addition, our equations are identical to those for the fluid dam-break classical problem, for which an analytic solution based on the method of characteristics is available in the planar case. This analogy has enabled us to validate our code. Another validation was obtained by recovering results obtained by Mangeney-Castelnau *et al.* (2004) for small-aspect-ratio columns without any 'rain'.

We investigated aspect ratios varying from 2 to 30, with four different initial values of the radius r_0. Comparisons with discrete simulations were made using the same dimensional values for the initial radius and height.

The choice of the initial condition, a cylinder of initial height $h_i = 0.1 r_0$, is justified by discrete simulations showing that the main part of the column collapses in free fall to a height comparable with the initial radius. We have investigated the influence of the thickness of this initial layer on the spreading dynamics. For $h_i \leqslant r_0$ the results are not affected by the initial condition, apart from the propagation of the front at short times. For $h_i \geqslant 1.5\, r_0$ the model fails to recover the correct behaviour, especially the scalings with a of the runout and final height.

2.3. *Discrete simulations*

In contrast to shallow-water equations, and continuum models in general, discrete simulation methods take into account the existence of the individual grains forming the granular media. Hypotheses on the nature of the interactions between the grains are thus necessary. Different models for contacts can be adopted, the discussion of which is beyond the scope of this paper.

The simulations discussed here were carried out using the Contact Dynamics (CD) algorithm (Moreau 1988; Jean 1994) in two dimensions. This method supposes perfectly rigid grains interacting through geometrical exclusion (ensuring that overlapping between grains is forbidden) and a simple Coulombic friction law. For the simulations presented in this paper, the value of the coefficient of friction between the grains μ_m was set to 1. Moreover, the coefficient of restitution for collisions e was set to 0.5. Typically, the aspect ratio of the column ranges from 2 to 15, and the number of grains ranges from 2000 to 8000. The columns were prepared by the random rain of grains into a cylinder. At the beginning of the experiment, the cylinder is removed and the grains fall in response to gravity. The bottom plane over which the grains spread is perfectly smooth, and the contacts between the grains and the plane have the same properties as the contacts between the grains themselves.

A detailed description of the CD simulations is presented elsewhere (Staron & Hinch 2005). Let us just mention that both the flow dynamics and the scaling laws obtained for the runout distance are in good agreement with the experimental results: $(r_\infty - r_0)/r_0 = 3.25 a^{0.7}$ for $a \gtrsim 2$.

3. Final runout distance and height, and dynamics of the flow

3.1. *Final runout and final central height*

One of the key points that the classical shallow-water model fails to reproduce is the scaling of the runout and final height. Indeed, classical shallow-water approaches give a runout distance increasing linearly with a, as expected from a simple friction behaviour. The runout distance and final central height obtained with the present

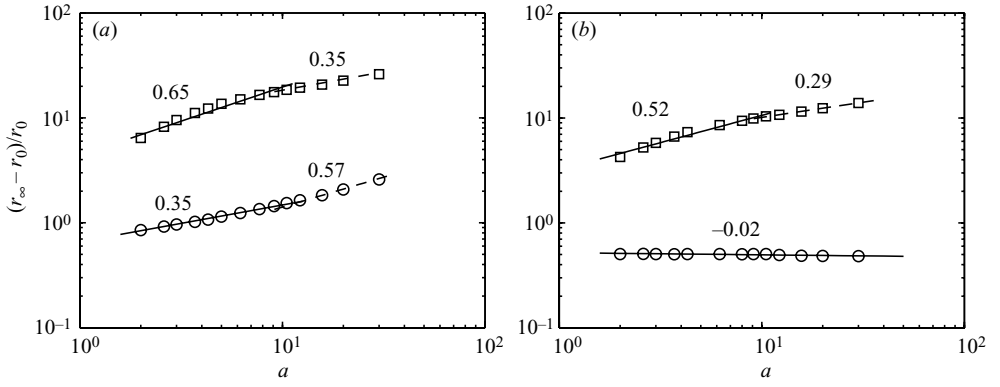

FIGURE 1. The runout distance $r_\infty - r_0$ (□) normalized by the initial radius r_0 and the final central height h_∞ (○) plotted as functions of the initial aspect ratio $a = h_0/r_0$ for planar (*a*) and axisymmetric (*b*) cases. The straight lines are power law a^n with index n taking the values indicated.

method are plotted figure 1 as a function of the aspect ratio a in both planar and axisymmetric cases. Two flow regimes clearly appear on these graphs.

For $2 \leqslant a \leqslant 10$, the runout scales as

$$(r_\infty - r_0)/r_0 = 4.4a^{0.65} \text{ in planar geometry,} \tag{3.1}$$

$$(r_\infty - r_0)/r_0 = 3.2a^{0.52} \text{ in axisymmetric geometry.} \tag{3.2}$$

The dependence in a^n appears to be in very good agreement with experimental results. Quasi-two-dimensional experiments give n equal to 2/3 (Lube *et al.* 2005) or 0.65 (Balmforth & Kerswell 2005). In axisymmetric geometry, both Lajeunesse *et al.* (2004) and Lube *et al.* (2004) find an exponent $n \approx 0.5$. For the first time, a continuum model is able to reproduce these experimental results in this range of a. Our prefactors 4.4 (planar) and 3.2 (axisymmetric) were obtained with a basal friction coefficient $\mu = 0.45$ and they overestimate the experimental results by a factor 2. We find that this prefactor varies approximately like $1/\mu$. This dependence on friction is compatible with observations by Lajeunesse *et al.* (2004) and Balmforth & Kerswell (2005) but not by Lube *et al.* (2004). In order to match the results obtained by Lube *et al.* (2005, 2004), our basal friction coefficient should be set to 0.9 in the planar, and 0.8 in the axisymmetric configuration. Such a high value of the basal friction coefficient might represent the dissipation occurring within the real flows due to vertical velocity variations, neglected in our plug-flow model.

In the second regime $a \geqslant 10$, the runout distance displays a different behaviour in both geometries:

$$(r_\infty - r_0)/r_0 = 8.2a^{0.35} \text{ in planar geometry,} \tag{3.3}$$

$$(r_\infty - r_0)/r_0 = 5.2a^{0.29} \text{ in axisymmetric geometry.} \tag{3.4}$$

This change is not observed in experiments; here our model fails to reproduce the correct runout for very tall columns. The discrepancy is less marked in the axisymmetric geometry.

The evolution of the final central height follows a similar pattern. In planar geometry,

$$h_\infty/r_0 = 0.66a^{0.35} \text{ for } 2 \leqslant a \leqslant 10, \tag{3.5}$$

$$h_\infty/r_0 = 0.38a^{0.57} \text{ for } a \geqslant 10, \tag{3.6}$$

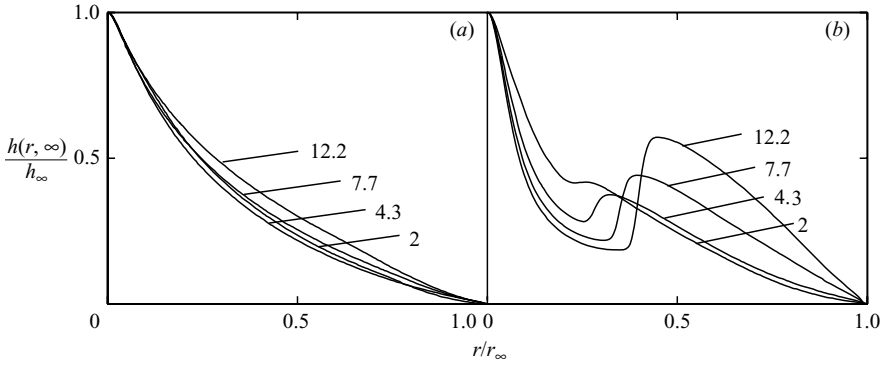

FIGURE 2. Shape of the deposit for different aspect ratios: (*a*) the planar case, (*b*) the axisymmetric. $h(r,\infty)$ is normalized by h_∞ and r by r_∞.

with a prefactor varying approximatively with μ. This should be compared with Lube *et al.*'s (2005) results who found for $a > 1.15$ a similar dependence with a: $h_\infty/r_0 = ka^{0.4}$ with $k = 1$ or 1.1 depending on the material used.

In the axisymmetric case, no change of the slope can be seen around $a = 10$. The final central height stays roughly constant, equal to a fraction of the initial radius over the whole range $2 \leqslant a \leqslant 30$: $h_\infty/r_0 = 0.52a^{-0.02}$. This quite surprising result matches the experimental law given by Lajeunesse *et al.* (2004) who found for $a > 0.74$ that $h_\infty/r_0 = 0.74$. Lube *et al.* (2004) found a weak dependence with $0.88a^{1/6}$ for $1.7 \leqslant a \leqslant 10$, followed by a decrease for higher a.

3.2. *Shape of the deposit*

In the planar case, the normalized deposit $h(r,\infty)/h_\infty$ versus r/r_∞ exhibits the universal shape of a long thin triangle independent of the initial aspect ratio for $a \leqslant 10$ (figure 2*a*). This interesting property has also been observed in two-dimensional experiments (Balmforth & Kerswell 2005). The $a = 12.2$ curve deviates slightly from the other curves. The universal shape enables us to relate the previous power laws for the final runout and the height using volume conservation $h_\infty r_\infty \propto h_0 r_0 = a r_0^2$. For $a < 10$, we find $h_\infty r_\infty \propto a^{1.0} r_0^2$ with the scaling laws 3.1 and 3.5, and $a^{0.92} r_0^2$ for $a \geqslant 10$ with equations 3.3 and 3.6. In experiments, Balmforth & Kerswell (2005) have observed that the final volume seems to increase by less than 10 % compared to the initial volume. This indicates that the averaged particle fraction remained roughly constant from the initial to the final states.

No universal shape is found in the axisymmetric case (figure 2*b*). The maximum height is reached in the centre of the deposit and a secondary maximum appears half-way along the runout. The height of this secondary maximum increases with a. The absence of a universal shape agrees with results from Lube *et al.* (2004). Although both Lajeunesse *et al.* (2004) and Lube *et al.* (2004) report only a slight secondary bump in their experiments for high aspect ratios ("Mexican hat shape", Lajeunesse *et al.* 2004), our numerical results greatly overestimate the bump. For $a \leqslant 10$, we recover the volume conservation in spite of the shape evolution: $h_\infty r_\infty^2 \propto a^{1.02} r_0^3$.

In both geometries, the final slope at the front is much lower than the slope that would be given by an internal angle of friction $\delta = \tan^{-1}(\mu) = 24^\circ$.

3.3. *Front propagation and duration of the flow*

One of the interesting observations made in the experiments is of the dynamics of the front, i.e. the moving edge of the evolving deposit. An initial phase of acceleration is

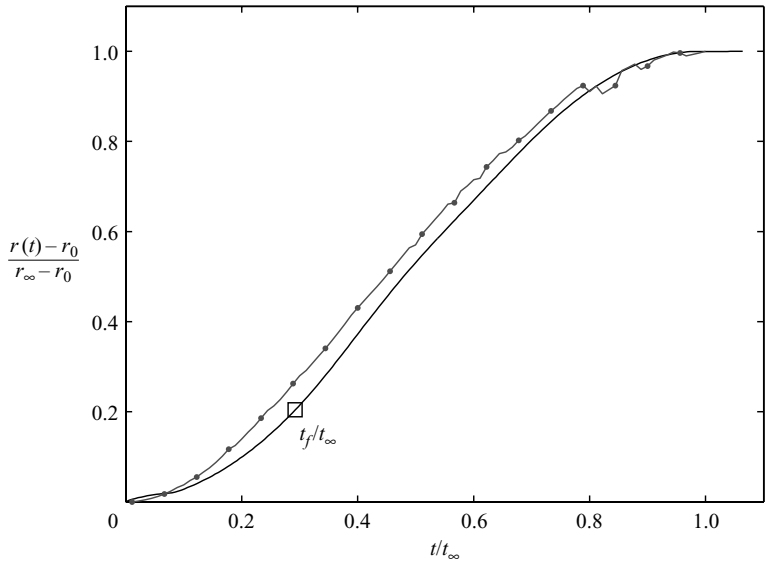

FIGURE 3. Front propagation in the planar case. $(r-r_0)/(r_\infty-r_0)$ is plotted as a function of t/t_∞. Shallow-water results (thick line) and discrete simulations results (thin line) are plotted for $a=7.7$. $r_\infty-r_0=16.03r_0$ for discrete simulation; $r_\infty-r_0=16.6r_0$ for shallow-water simulations and $t_\infty=8.36\sqrt{2r_0/g}$ (discrete) or $9.4\sqrt{2r_0/g}$ (shallow-water). The square marks the end of the free fall t_f.

followed by a long phase of constant velocity, and finally a short phase of abrupt deceleration before the flow stops. Once the front has stopped most of the grains are stationary, and only minor surface flows involving a few particles are observed. Figure 3 displays the results obtained with our model and with discrete simulations for the same initial condition of $a=7.7$. Although the final time t_∞ and runout distance r_∞ are slightly higher for this a in the shallow-water calculation, the agreement between the two is quite good. The shallow-water model reproduces a phase of acceleration followed by a phase of constant velocity. This constant-velocity phase results from a balance between deceleration due to basal friction and acceleration due to the slope $\partial h/\partial r$. A final short period of deceleration during which frictional effects overcome the flow leads to the final full stop of the front at $t=t_\infty$. One should note that this stop is well-defined, contrary to what would be observed in classical fluid dynamics. The duration of the constant-velocity and the deceleration phases are quite similar in our shallow-water calculation and in the simulations, and the final runout is almost identical.

In the short initial phase, the discrete simulation flow accelerates in agreement with experiments. The shallow-water calculation has a small non-zero initial velocity due to the initial condition $h_i=0.1r_0$, and then has a short phase of constant acceleration.

In axisymmetric geometry, the front propagation follows the same behaviour. After an initial acceleration phase, the velocity remains constant during the main part of the flow, and then a brief phase of deceleration leads to the sudden stop of the mass.

The duration of the numerical flow $t_\infty/\sqrt{2r_0/g}$ as a function of the aspect ratio a is displayed figure 4 for planar and axisymmetric calculations. The evolution is quite similar in the two geometries:

$$t_\infty/\sqrt{2r_0/g}=4.35a^{0.36} \text{ in planar geometry,} \tag{3.7}$$

$$t_\infty/\sqrt{2r_0/g}=3.75a^{0.33} \text{ in axisymmetric.} \tag{3.8}$$

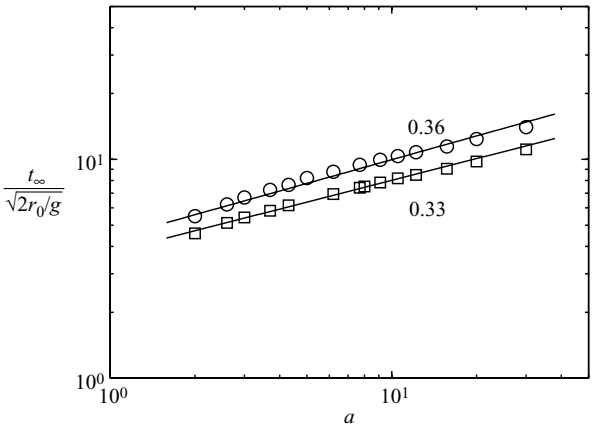

FIGURE 4. Duration of the runout $t_\infty/\sqrt{2r_0/g}$ as a function of a in planar (○) and axisymmetric (□) experiments. The straight lines are power law a^n with index n taking the values indicated.

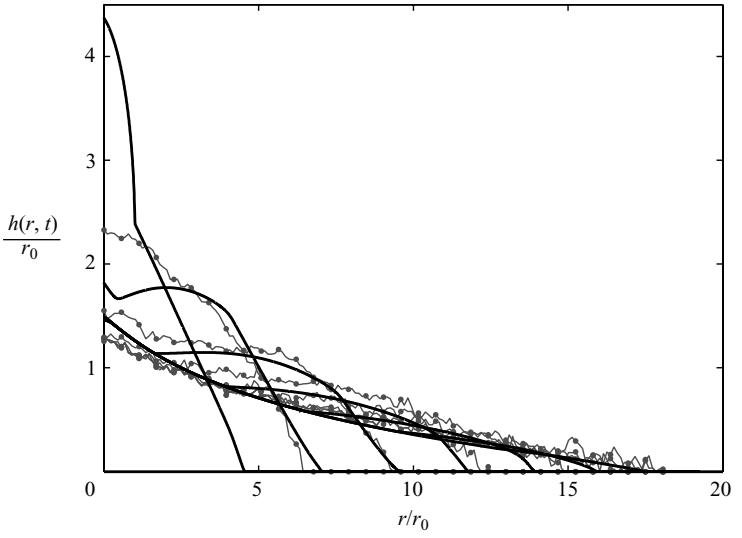

FIGURE 5. Time evolution of the deposits. Rescaled shape h/r_0 as a function of r/r_0 for $a = 9.1$. Profiles are plotted at times $t/t_\infty = 0.3(0.1)1.0$. Thick and thin lines represent shallow-water and discrete simulations respectively.

This dependence is continuous through $a = 10$ contrary to the previous changes in slope observed in figure 1 for the runout and final height. The power-law behaviour seems to be almost independent of the geometry, as observed in experiments by Lube *et al.* (2004, 2005). In the experiments, however, $a^{1/2}$ is found instead of our $a^{1/3}$, making t_∞ proportional to the free-fall time $\sqrt{2h_0/g}$. We thus underestimate the duration of the flow, although the prefactors produce less difference in the range of the experiments.

4. Comparison with discrete simulations

4.1. *Height profiles*

Figure 5 displays the evolution of the height profiles in time for $a = 9.1$. The profiles given by shallow-water calculations show a reasonably good agreement with the

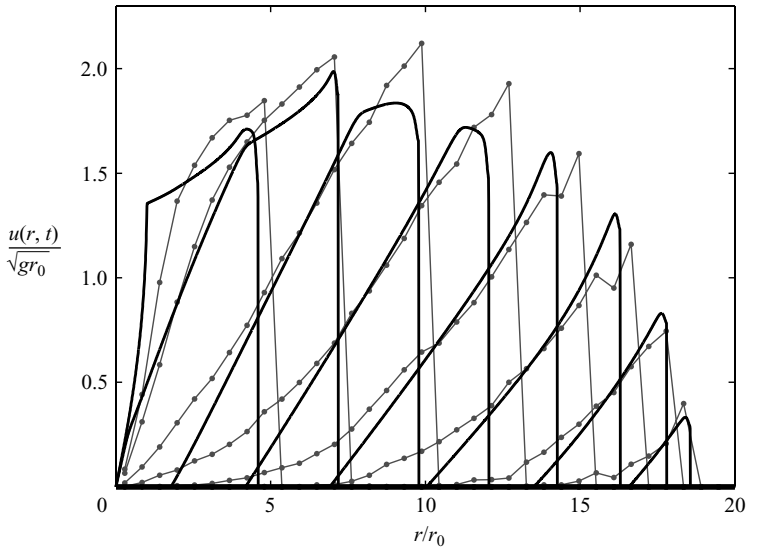

FIGURE 6. Time evolution of the velocity profile $u(r,t)/\sqrt{gr_0}$ as a function of r/r_0 for $a=9.1$ at the same times and with the same notation as figure 5.

discrete simulations. The agreement improves in time up to the final stage where the two profiles are remarkably similar.

At the earliest time $t=0.3t_\infty=t_f$, the shallow-water results show an accumulation of mass which has not yet been accelerated away as in the discrete simulations. This is a feature of the shallow-water model where acceleration can only occur with slopes whereas in experiments or discrete simulations material can be pushed away from the initial release zone.

The slope at the nose seems to be constant in time during most of the flow $t>t_f$. This reflects the constant velocity observed in figure 3 where acceleration due to the constant slope is exactly cancelled by deceleration due to the constant friction.

4.2. *Velocity profiles*

The evolution of the velocity profile in the spreading layer is readily available in simulations but is quite difficult to measure experimentally. It is displayed figure 6 for both shallow-water and discrete simulations results; for the discrete simulations, the horizontal velocity has been depth-averaged. These results are in surprisingly good agreement considering the rough hypothesis of plug-flow velocity in the shallow-water model. Figure 6 shows that the central part of the material remains stationary. The velocity then increases linearly to a maximum, reached very close to the front. This maximum remains roughly constant for a long time, in agreement with the constant velocity of the front observed figure 3. The profile indicates that the material is stretched during the whole flow. This figure also shows that the stopping front, dividing the central stationary part from the outer moving material, propagates outwards. This feature has been observed in experiments (Lube *et al.* 2005).

5. Energy budget

The initial potential energy in the tall column is $E_0=\frac{1}{2}\pi g r_0^2 h_0^2$ (axisymmetric) and $\frac{1}{2}g r_0 h_0^2$ (planar). If one were to use the shallow-water equations to describe the entire collapse starting from this initial tall and very much non-shallow column, then the

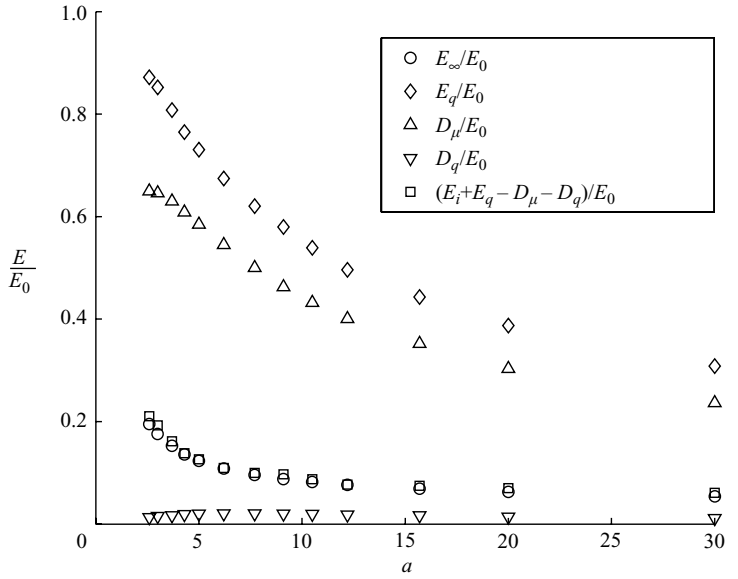

FIGURE 7. Energy balance for different aspect ratios. The data are normalized by the full potential energy of the initial column E_0. The final energy E_∞/E_0 ($\bigcirc$) is equal to the energy balance $(E_q + E_i - D_\mu - D_q)/E_0$ ($\square$), where E_i is the initial potential energy (not plotted), E_q ($\diamondsuit$) is the potential energy due to the mass addition, D_μ ($\triangle$) is the frictional dissipation and D_q ($\triangledown$) the dissipation due to the mass addition.

initial potential energy is quickly converted by the equations into horizontal kinetic energy with velocities $O(\sqrt{gh_0})$. The sideways flow then decelerates at μg to run out to a distance $O(h_0/\mu)$, i.e. $(r_\infty - r_0)/r_0 \propto a^1$, which is too far. Hence some energy must be lost by another mechanism.

To understand the energetics of our modified version of shallow-water theory, we first derive the local energy equation from equations (2.1) and (2.2) for the conservation of mass and momentum,

$$\frac{\partial}{\partial t}\left(\frac{1}{2}hu^2 + \frac{K}{2}gh^2\right) + \frac{1}{r}\frac{\partial}{\partial r}\left(rhu\left(\frac{1}{2}u^2 + Kgh\right)\right) = qKgh - \mu ghu - \frac{1}{2}qu^2, \quad (5.1)$$

for the axisymmetric case and omitting the two metric factors of r in the planar case. We see on the right-hand side that potential energy is introduced by the rain, work is done against basal friction, and in the final term energy is dissipated when the rain with no horizontal velocity is mixed instantaneously into the sideways flow. One might have anticipated that this last term was the key additional dissipation required to shorten the runout distance, but we see in figure 7 that its integrated effect

$$D_q = \int_0^{t_f}\int_0^{r_0} \frac{1}{2}qu^2 \,\mathrm{d}r\,\mathrm{d}t$$

(in the planar case) is small, less that 5 % of the initial potential energy E_0 in the tall column.

The important feature of our 'rain' modification turns out to be that the supply of potential energy to drive the sideways flow is only

$$E_q = \int_0^{t_f}\int_0^{r_0} qKgh \,\mathrm{d}r\,\mathrm{d}t$$

(in the planar case). This is much lower that the initial potential energy in the tall column, because the 'rain' is fed in at the height $h(r, t)$ which is always significantly lower than $\frac{1}{2}h_0$. Our modified version of the shallow-water model therefore allows the tall column to fall freely under gravity in so far as the mass input q is concerned, but then says that the vertical kinetic energy is fully dissipated when the grains impact on the base, leaving nothing to input into horizontal kinetic energy in the sideways flow.

The key question addressed by our modified version is now seen to be the piling up caused by the 'rain' which is necessary to accelerate the grains away from the base of the column, with important differences in this evacuation between axisymmetric and planar geometries.

Figure 7 shows the various components in the energy budget for the collapse of planar columns of different aspect ratios. We see that the supply of potential energy E_q as a fraction of the total potential energy in the initial tall column E_0 decreases with aspect ratio, dropping to around 30 % by $a = 30$. The dissipation due to the mixing of the rain into the horizontal flow D_q is negligible compared with E_0, while the total dissipation by the basal friction

$$D_\mu = \int_0^{t_\infty} \int_0^{r(t)} \mu g h u \, \mathrm{d}r \, \mathrm{d}t$$

(in the planar case) removes most of the supplied energy, leaving the final potential energy when the flow has stopped

$$E_\infty = \int_0^{r_\infty} \frac{K}{2} g h^2 \, \mathrm{d}r \, \mathrm{d}t$$

(in the planar case) at $t = t_\infty$. We have checked that our numerical code satisfied the overall energy budget $E_\infty = E_i + E_q - D_\mu - D_q$, where E_i is the potential energy in our initial condition $h_i = 0.1 r_0$ in $r < r_o$.

6. Conclusion

Our modified shallow-water model is the first continuum model to reproduce, for not too high aspect ratios $a < 10$, the correct runout dependence, $a^{1/2}$ and $a^{2/3}$, in both axisymmetric and planar geometries. The final shape of the deposit is good in planar geometry, where a universal shape is also found in experiments and discrete simulations. As in the experiments, we find no universal shape in axisymmetric flow, although our 'Mexican hat' shape is more pronounced. In both geometries, the front runs at a constant velocity for most of the time, as in discrete simulations and experiments. The planar shape and the velocity profiles evolve in time in agreement with discrete simulations. The duration of the runout, however, is shorter than in the experiments of Lube *et al.* (2004, 2005).

The key feature of our model is that a substantial part of the initial potential energy in the tall column E_0 is not supplied by the 'rain' in E_q, because we assume all the vertical kinetic energy of the free-fall is lost on impact with the plane.

Our model fails for high aspect ratios. One explanation could be that the shallow-water equations cannot push the grains away from the raining area with pressure but must accelerate the flow away by having a surface slope. It seems that at high aspect ratio this acceleration cannot keep up with the increasing mass flux in the rain, and instead a temporary high central peak occurs, as in figure 5 at $t/t_\infty = 0.3$. However, if such an averaged continuum model cannot capture the whole dynamics of the flow,

it is interesting that it is able to recover many features with the simplest ingredients: basal friction and mass addition.

REFERENCES

Balmforth, N. J. & Kerswell, R. R. 2005 Granular collapse in two dimensions. *J. Fluid Mech.* **538**, 399–428.

Gray, J., Tai, Y.-C. & Noelle, S. 2003 Shock waves, dead zones and particle-free regions in rapid granular free-surface flows. *J. Fluid Mech.* **491**, 161–181.

Gray, J. M. N. T., Wieland, M. & Hutter, K. 1999 Gravity-driven free surface flow of granular avalanches over complex basal topography. *Proc. R. Soc. Lond.* **445**, 1841–1874.

Hirsch, C. 1988 *Numerical Computation of Internal and External Flows*, vol. 2. Vrije Universiteit Brussel, Belgium: John Wiley & Sons.

Jean, M. 1994 *Frictionnal Contact in Collections of Rigid or Deformable Bodies: Numerical Simulation of Geomaterial Motions*. Elsevier.

Lajeunesse, E., Mangeney-Castelnau, A. & Vilotte, J. 2004 Spreading of a granular mass on an horizontal plane. *Phys. Fluids* **16**, 2371–2381.

Lube, G., Huppert, H. E., Sparks, R. & Freundt, A. 2005 Collapses of granular columns. *Phys. Rev.* E **72**, 04130.

Lube, G., Huppert, H. E., Sparks, R. & Hallworth, M. 2004 Axisymmetric collapses of granular columns. *J. Fluid Mech.* **508**, 175–199.

Mangeney-Castelnau, A., Bouchut, F., Lajeunesse, E., Aubertin, A., Vilotte, J. & Pirulli, M. 2004 On the use of Saint-Venant equations for simulating the spreading of a granular mass. *J. Geophys. Res.* **199**, 177–215.

Moreau, J. J. 1988 Unilateral contact and dry friction in finite freedom dynamics. In *Nonsmooth Mechanics and Applications* (ed. J. J. Moreau & P. D. Panagiotopoulos). Springer.

Pouliquen, O. & Forterre, Y. 2002 Friction law for dense granular flows: application to the motion of a mass down a rough inclined plane. *J. Fluid Mech.* **453**, 133–151.

Savage, S. & Hutter, K. 1989 The motion of a finite mass of granuar material down a rough incline. *J. Fluid Mech.* **199**, 177–215.

Staron, L. & Hinch, E. J. 2005 Study of the collapse of granular columns using two-dimensional discrete-grain simulation. *J. Fluid Mech.* **545**, 1–27.

Tai, Y.-C., Noelle, S., Gray, J. M. N. T. & Hutter, K. 2002 Shock capturing and front tracking methods for granular avalanches. *J. Comput. Phys.* **175**, 269–301.